CHAPTER

Measurement of cell traction forces with ImageJ

15

Jean-Louis Martiel*,[1], Aldo Leal*, Laetitia Kurzawa*, Martial Balland[§], Irene Wang[§], Timothée Vignaud*, Qingzong Tseng*, Manuel Théry*,[¶,1]

*CytoMorpho Lab, Institut de Recherche en Technologie et Science pour le Vivant, LPCV/UMR5168, CEA/INRA/CNRS/Univ. Grenoble-Alpes, Grenoble, France

[§]Laboratoire Interdisciplinaire de Physique, UMR 5588, CNRS/Univ. Grenoble-Alpes, Grenoble, France

[¶]CytoMorpho Lab, Hopital Saint Louis, Institut Universitaire d'Hematologie, U1160, INSERM/AP-HP/Université Paris Diderot, Paris, France

[1]Corresponding authors: E-mail: jean-louis.martiel@cea.fr; manuel.thery@cea.fr

CHAPTER OUTLINE

Methods in Cell Biology, Volume 125, ISSN 0091-679X, http://dx.doi.org/10.1016/bs.mcb.2014.10.008

Abstract

The quantification of cell traction forces requires three key steps: cell plating on a deformable substrate, measurement of substrate deformation, and the numerical estimation of the corresponding cell traction forces. The computing steps to measure gel deformation and estimate the force field have somehow limited the adoption of this method in cell biology labs. Here we propose a set of ImageJ plug-ins so that every lab equipped with a fluorescent microscope can measure cell traction forces.

INTRODUCTION

In 1997, Pelham and Wang showed how collagen-coated polyacrylamide hydrogels can be used to culture cells on substrates of controlled stiffness (Pelham & Wang, 1997). In 1999, Dembo and Wang showed how the measurement of polyacrylamide hydrogels deformation can be used to infer the corresponding cell traction force field (Dembo & Wang, 1999). Since then, this pioneer method has been steadily optimized on both the experimental and the numerical sides making the traction force measurement a faster and more accurate method (Butler, Tolić-Nørrelykke, Fabry, & Fredberg, 2002; Sabass, Gardel, Waterman, & Schwarz, 2008; Stricker, Sabass, Schwarz, & Gardel, 2010). The Extra Cellular Matrix (ECM) coating on the polyacrylamide is now more homogenous and reproducible (Rape, Guo, & Wang, 2011). The numerical estimation of the force field in the Fourier space has considerably reduced the computing time without great compromise on method precision (Butler et al., 2002). The method seems now mature enough to become a routine technique in any laboratory. As we were new incomers in the field, we spent some time to optimize the technical steps in our hands (Schiller et al., 2013; Tseng et al., 2011, 2012) and make the code usable by any lab members. We selected the simplest and most reliable method to graft ECM proteins on polyacrylamide gels and optimized the treatment of images so that it can be handled using ImageJ on a personal computer. To that end we wrote few ImageJ/Fiji macros that are described at the end of this chapter.

The measurement of traction forces exerted by adhering cells involves several steps: (1) gel preparation and cell culture, (2) image acquisition and processing, (3) measurement of the gel deformation by particle image velocimetry (PIV), and (4) force measurement itself. Each step is associated with some key parameters that have to be experimentally controlled or numerically defined (Figure 1).

In the following sections, we will first very briefly introduce the theoretical basis of gel deformation in response to superficial traction forces so that readers can be familiar with the concept used thereafter (Section 1); then, we will present and discuss the critical parameters of the measurement method. Experimental parameters will be detailed in Section 2 and numerical parameters in Section 3. A detailed protocol of ECM-coated polyacrylamide hydrogel manufacturing will be

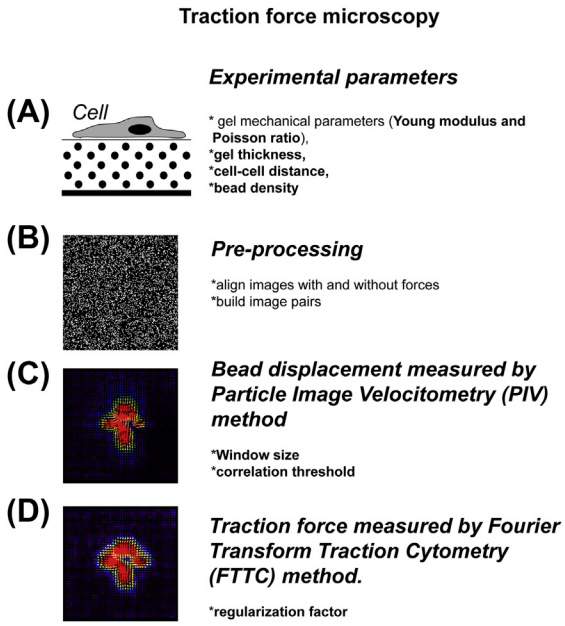

FIGURE 1 Layout of the force measurement method.

Cells plated on elastic gels exert forces that deform gel and induce the displacement of fluorescent beads included in the gel (A). Pairs of images with force and without force are created, aligned, and cropped (B). Using the ImageJ plug-in PIV, get the bead displacement (C). Finally, the plug-in FTTC is used to measure the traction force, exerted by the cell and which is responsible of gel deformation and bead displacement (D). (See color plate)

explained in Section 4. Finally, image acquisition and ImageJ macros will be described in Sections 5 and 6.

1. FORCE MEASUREMENT PRINCIPLE

Different physical methods have been developed to measure the magnitude and the direction of forces produced by cells. These methods use either elastic micropillars (Gupta et al., 2014 [Chapter 16 of this volume]) or elastic gels and traction force microscopy (Plotnikov, Sabass, Schwarz, & Waterman, 2014; Serra-Picamal, Conte, Sunyer, Muñoz, & Trepat, 2014 [Chapter 17 of this volume]). These methods are also adapted to natural elastic fibers (collagen) using pseudo-speckle microscopy to quantify the fiber contraction in vivo (Kopansaka et al., 2014 [Chapter 19 of this volume]). However, force measurement requires a careful analysis of the physical models/methods behind the experimental results and the quantification of forces. In addition, the writing of analysis software can be a limiting step in the adoption of these methods.

ImageJ platform is a convenient way to share and make available analysis tools. Here, we present ImageJ plug-ins and macro and attempt to justify all underlying assumptions during data processing.

A cell attached to a soft gel produces forces that deform the gel, as schematized in Figure 2. The gel deformation is measured by the technique of PIV, which tracks fiducial markers (fluorescent beads). This technique is based on the correlation of

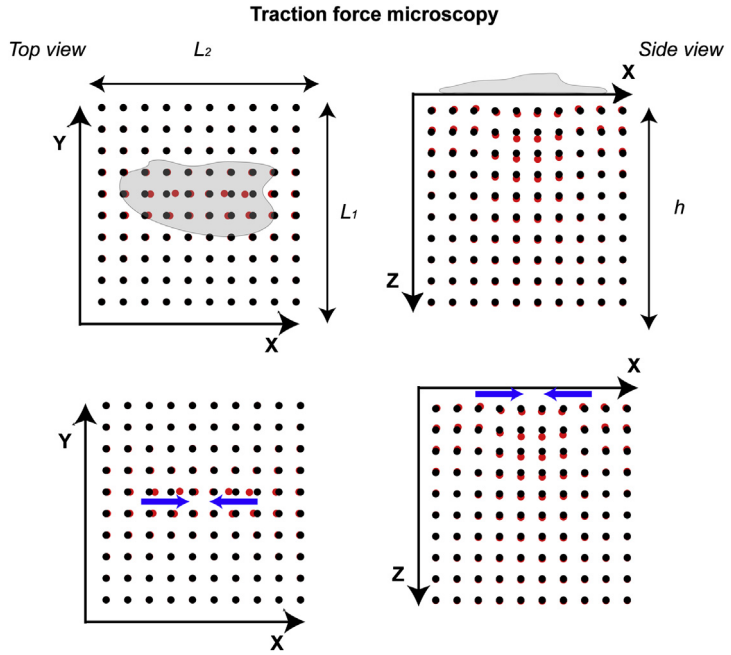

FIGURE 2 Bead displacement and force measurement.

The bead displacement is measured by the change of bead spatial position between a reference configuration without force (black dots, all panels) and in presence of force (red dots (gray in print versions), all panels). Equations of linear elasticity predict the displacement as a function of (1) the force exerted by the cell (blue arrows (dark gray in print versions), bottom row) and (2) the gel mechanical characteristics (Young modulus and Poisson ratio). However, the use of equations valid for an infinite half space requires that the bead displacement is zero at the bottom of the gel (right column panels) or away from the force application points (left column panels). In consequence, for typical gel rigidity in the range 500–50,000 Pa and forces below 100 nN, the gel thickness (parameter h) and intercell distance (parameters L_1 and L_2) should be of the order of 100 μm. Bead displacement is simulated for a Young modulus of 35,000 Pa, for a cubic gel (dimension $140 \times 140 \times 140$ μm) and a horizontal force of 0.1 nN (symbolized by the blue arrows (dark gray in print versions)). The maximal displacement observed in the horizontal (X,Y) plane is ~6 and 2 μm in the (X,Z) vertical plane.

two interrogation windows, one taken in the image without force and the other taken in the image with force (here, with the cell). The displacement of fiducial markers is determined by looking for the maximal correlation of the fluorescence between the two interrogation windows.

Here, we assume that polyacrylamide gels are homogenous, isotropic, and that their elastic response is linear with respect to the applied force. In consequence, the force $\mathbf{f}(\mathbf{x})$, where $\mathbf{x} = (x, y)$ represent a point at the surface of the gel, is related to the displacement $\mathbf{u}(\mathbf{x})$ through a linear relation.

$$\mathbf{u}(\mathbf{x}) = \int \sum_n \mathbf{G}(\mathbf{x} - \mathbf{y})\mathbf{f}_n(\mathbf{y})d\mathbf{y}, \tag{1}$$

where $\mathbf{f}_n(\mathbf{x})$ is the nth force point. Given the displacement field $\mathbf{u}$, measured by the PIV method and the Green function $\mathbf{G}$, Eqn (1) should be inverted to give the traction force $\mathbf{f}$. One can use the Boussinesq function, valid for a semi-infinite half space

$$\mathbf{G}(\mathbf{x}) = \frac{(1+\nu)}{\pi Y r^3}\begin{pmatrix} (1-\nu)r^2 + \nu x^2 & \nu xy \\ \nu xy & (1-\nu)r^2 + \nu y^2 \end{pmatrix}, \tag{2}$$

with $r = |\mathbf{x}|$, Y is the Young modulus (Pa) and ν the Poisson ratio (no dimensions). From Eqns (1) and (2), one gets a simple approximation of the displacement magnitude given the gel rigidity (Y), the force magnitude, f, and the distance from the force application point, r

$$u(r) \approx \frac{f}{Yr} \tag{3}$$

Equation (3) can be used as rule of thumb to guess the order of magnitude of displacement for a given Y and force. For example, if $Y = 10{,}000$ Pa and $f = 10$ nN, one expects a displacement of 1 μm at 1 μm of the application point of the force.

The next step in the analysis is the inversion of Eqn (1), knowing the gel rigidity (Y) and the gel displacement, $\mathbf{u}$; this latter quantity being determined by PIV using two images of the same gel, one with cells and the other without cells.

Basically, inverting Eqns (1) and (2) could be achieved by a finite element approach but with a high cost in terms of numerical simulations and software development. In consequence, we use methods based on the Fourier transform traction cytometry (FTTC). This method takes advantage of the linearity of Eqn (1) to change the integral in the space domain into a large system of linear equations in the Fourier domain (Sabass et al., 2008). Later, the basic FFTC has been modified to match the constrains of experiments in which the cell-to-cell distance is not infinite (Trepat et al., 2009; Tambe et al., 2013). In this study, we limited our analysis to the case of semi-infinite gels and isolated cells.

This linear system in the Fourier space is an ill-posed problem. It can have several solutions, which can be more or less realistic in cell biology. For example, it is reasonable to assume that cells do not push and pull at two very close sites. Solutions corresponding to this type of behavior can be ignored. Therefore, we look for a force $\mathbf{f}$ by minimizing

$$J = |\mathbf{G}\cdot\mathbf{f} - \mathbf{u}|^2 + \lambda^2|\mathbf{f}|^2 \quad (4)$$

where **f** and **u** are the force and the displacement field, respectively, **G** is the operator obtained from the Green function (Eqns (1) and (2)), and λ is a regularization factor; λ governs the relative importance of experimental data (first term in Eqn (4)) and the amplitude of the solution (second term) during minimization of *J*. By reducing the amplitude of **f** (second term in Eqn (4)), the contribution of high frequencies in the Fourier domain is eliminated (in this analysis high-frequency signal is assimilated to noise) and we get a smooth solution of Eqn (1) given the measured displacement **u**.

2. CRITICAL EXPERIMENTAL PARAMETERS

Force traction measurement relies on a series of assumptions on the properties of the gel (homogenous, linear response, rigidity) and on the magnitude of the force developed by cells. It is also limited by numerical parameters used for image analysis (interrogation window size…). In this section and the next one, we will estimate the best range for the different parameters.

- Gel thickness and intercell distance

Equation (2) is valid for a semi-infinite half space. In practical terms, this means that the intercell distance (parameters L_1 and L_2, Figure 2, top left panel) and the gel thickness (parameter *h*, Figure 2, top right panel and Table 1) should be large. Given the expected force magnitude (1−10 nN) and gel rigidity (10 kPa), Eqn (3) predicts that the displacement is negligible (∼0.01 to 0.1 μm) at a distance of 100 μm. This latter value can be used in gel preparation (parameter *h*) or cell seeding (parameters L_1 and L_2).

- Gel rigidity and range of deformation

Equations (1) and (2) are valid in the limit of small and linear gel deformations; however, the force-induced gel deformation should be larger than the random displacements of fluorescent beads in the gel or gel swelling during image acquisition. In consequence, the gel rigidity (parameter *Y* in Eqn (2)) should be experimentally tuned so that the expected displacement lies in the range 0.1−10 μm (see Eqn (3)). Using different force magnitude and Young modulus parameters, we computed the maximal displacement at 10 μm of the point where the force is applied (Figure 3 and Table 1). We predict three domains of interest. In domain A, the displacement is too large; hence, the assumption of small gel deformation is not valid for this combination of force rigidity. In domain C, gel deformation is below or equal to 0.1 μm, yielding a signal-to-noise ratio close to 1. Only in domain B will we find optimal combination of gel rigidity and force magnitude that permits the use of Eqn (2) (FTTC method).

Table 1 Experimental and Numerical Parameters Used during Force Measurement

Experimental Conditions	Reason	Proposed Bound or Typical Value Used	Importance
Bead density should be small	Equations are valid for a homogenous medium. Beads should represent less than 10% of the volume fraction	5–10% in volume fraction	+
Gel thickness	Equations are valid for an infinite half space	Gel thickness $\sim$100 μm	++
Intercell distance	If cells are close (or contiguous), it is (almost) impossible to distinguish the contribution of each cell to the displacement	Intercell distance of $\sim$50 μm	++
Small gel deformation	Equations are valid in the limit of small deformations of continuous medium	Gel deformation <5% (deformation: ratio of the difference between deformed/resting distance over the resting distance)	+++
Bead-background contrast	Displacement is measured by correlation of the fluorescence in sub-images (PIV)	Highest possible contrast	++++
Bead image quality	Ideally, beads in the two images (with and without cells) should be identifiable (e.g., no pop up of new beads between with and without force images)		++++
Force magnitude/gel rigidity	The bead displacement scales with the traction force and is inversely proportional to the gel Young modulus	Adapt the gel rigidity to the expected force magnitude developed by cells	++++

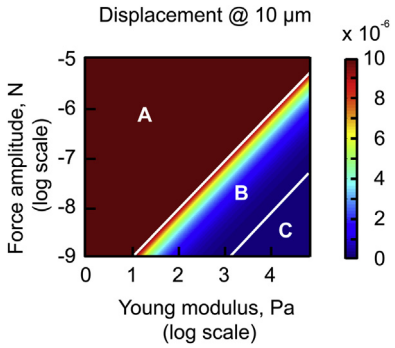

FIGURE 3 Force magnitude and gel rigidity.

The bead displacement scales with the traction force and is inversely proportional to the gel Young modulus. In consequence, the gel rigidity should be adapted to the expected force exerted by cells. Here, we use the exact equations for elastic medium to predict the displacement at 10 μm from the force point for different Young modulus (horizontal axis) and force magnitude (vertical axis) (see Eqn (2), main text). In domain A, the displacement is larger than 10 μm and cannot be accounted for by linear deformation theory. In domain C, the bead displacement is undetectable (below or equal to 0.1 μm) and cannot be used in force measurement. Only in domain B can the bead displacement be useful to predict correctly the force. In conclusion, the combination of gel rigidity (Young modulus) and expected force magnitude lies close to the boundary between domains A and B. To save the displacement scaling (color code on the right), we plot displacement less or equal to 10 μm (this is important in domain A). (See color plate)

- Image size

Images of gel deformation are acquired with the source of the force (i.e., the cell) at the image center. Fiducial markers at the margins of the image, away from the application of force, should be immobile. Given the expected force magnitude and gel rigidity, Eqn (3) would help in determining the image size and microscope magnification.

3. CRITICAL NUMERICAL PARAMETERS

The quality of displacement and force measured by PIV and FTTC depends on three parameters, namely, the size of the interrogation window (PIV), the correlation threshold (PIV), and the regularization factor (FTTC). To illustrate their role and determine the optimal parameter set, we generated images representing bead displacement, denoted $\mathbf{u}_a$, in an elastic gel with a known rigidity and applied force, denoted $\mathbf{f}_a$, with the help of Eqns (1)–(2). Then, from two images, one representing the relaxed state and the other the bead displaced by the gel deformation, we determined the displacement field $\mathbf{u}_{exp}$ and the force $\mathbf{f}_{exp}$ with the help of the ImageJ plugins for different values of the three parameters (Figure 4).

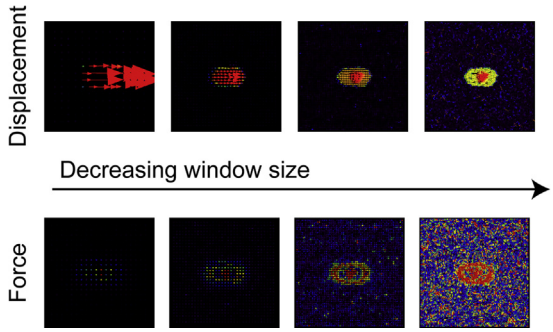

FIGURE 4 Qualitative role of the window size (last interrogation window in PIV method).

We generated artificial images corresponding to the application of a 10-nN horizontal force and bead density of 5000 per 512 × 512 pixels image. The size of the last window in PIV analysis is decreased (30, 20, 10, and 5 pixel width, from left to right). The optimal prediction for both the displacement (top row) and the force (bottom row) is obtained for a 20-pixel width interrogation window. (See color plate)

The displacement of beads, $\mathbf{u}_{exp}$, which is assumed to follow the gel deformation, is determined for all possible interrogation windows in the image. The PIV relies on a correlation threshold (usually 0.6) above which the displacement between interrogation windows (i.e., the pixel shift between images) is considered to represent an actual bead displacement. Note that the size (in pixels) of the interrogation windows determines the sampling of the true gel deformation. In addition, parameters, such as the number of beads or the maximal possible shift between interrogation windows, are important factors that control the quality of the measure. Finally, we computed the distance between $\mathbf{u}_a$ and $\mathbf{u}_{exp}$ (respectively, $\mathbf{f}_a$ and $\mathbf{f}_{exp}$) to determine the optimal parameter set for the method.

- Interrogation window size (PIV)

First, we generated the bead displacement in response to 10 nN force applied at the image center (Figure 4 and Table 1). Then, we used PIV with different window size (30, 20, 10, and 5 pixels width, left to right; correlation threshold: 0.6) and FTTC ($\lambda = 8.10^{-11}$) to predict the displacement (top row) and force (bottom row). The best displacement-force prediction is obtained for 20 pixel interrogation window (leftmost panels in Figure 4).

- Bead density

In Figure 5 (and Table 1), we present the error for displacement (left panel) or force (right panel) for different bead densities (assuming a 2D distribution of fiducial markers) and interrogation window sizes. The optimal combination of parameters corresponds to a minimal number of beads per interrogation window of 4−5 (left and right panels, Figure 5) where the error curve is minimal. It is easy to understand

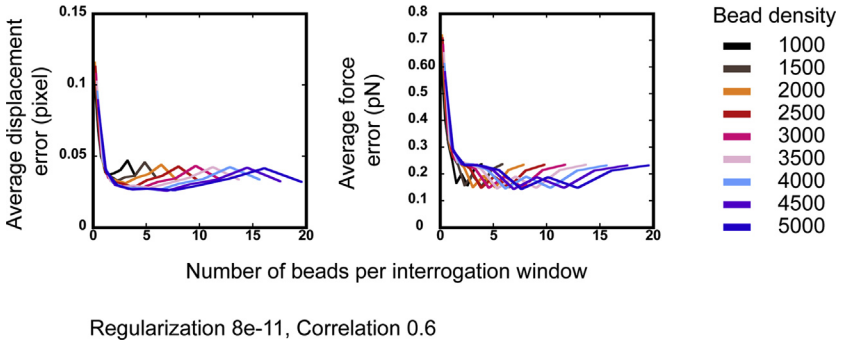

FIGURE 5 Error on displacement and force estimation: role of the interrogation window size and bead density.

We used synthetic images simulating the application of a force of 10 nN (middle in the image) for different bead density (indicated by the color code). The actual bead displacement, predicted by the (linear) equations for an elastic medium ($Y = 35{,}000$ Pa), is compared against the displacement obtained through the PIV method. The number of beads in the image is the critical parameter that controls the error in displacement (left panel) or in the force (right panel). Other parameters, such as the correlation threshold, the regularization factor, have less importance. In conclusion, the number of beads in the last interrogation window used in PIV should be at least four (left panel) to minimize the error in displacement measurement.

the lower limit of four beads per window: The change in fluorescence due to bead displacement is too small to be detected as a signal by the PIV procedure. Conversely, a change in fluorescence resulting from bead displacement in images with a high density of beads would be hard to detect just by looking at the relative change in fluorescence between interrogation windows. In addition, high-density images makes bead tracking (identification of the same bead) from without-force to with-force images difficult. In conclusion, all the error curves present a shallow minimum for the error (Figure 5).

- Correlation threshold and regularization factor

Using synthetic images, we also analyzed the role of the correlation threshold (PIV method, Figure 6 and Table 1) and regularization factor (FTTC method, Figure 7). In all cases, we used a 512×512 pixel image with a bead density of 5000 beads per image. The output, for both displacement (left panel) and force (right panel) is almost independent on the actual value for the correlation threshold. However, for threshold smaller than 0.5, we observed a drop in the quality of displacement prediction. For threshold values of 0.4 and 0.3, the displacement prediction gives poor estimation of the force (simulations not shown) and, therefore, cannot be used. Using the same technique of synthetic images, we also analyzed the role

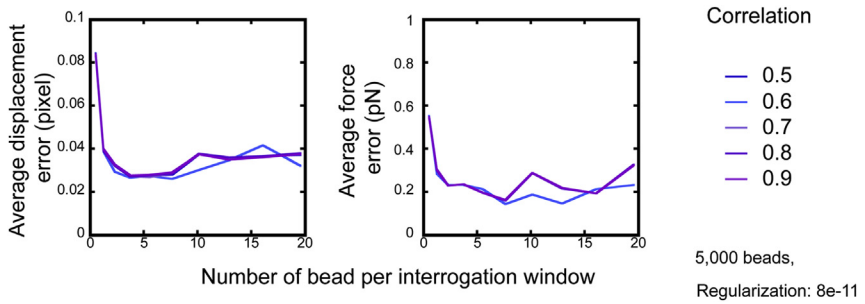

FIGURE 6 Role of correlation threshold.

In the same numerical study, we vary the correlation threshold from 0.6 to 0.9 (color code on the right). The errors both in displacement (left panel) and in force (right panel) measurement are not affected by this factor. In addition, these results confirm the optimal value of at least four beads per interrogation window obtained in Figure 4.

of the regularization factor (Figure 7). For a critical density of five beads per interrogation window, the prediction of the force is not affected by the exact value of λ. However, at low bead density, this parameter is crucial, since we observe a large error for low λ (Figure 7).

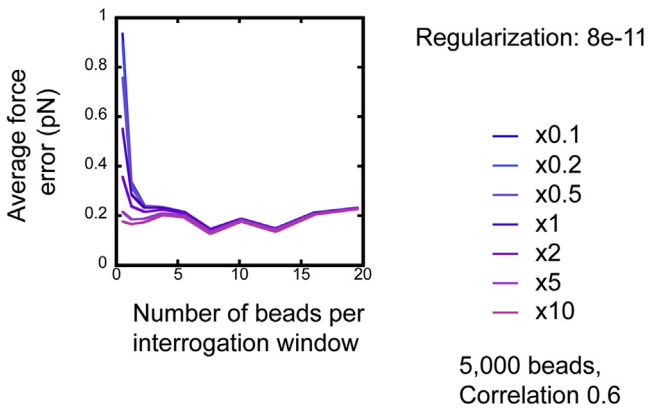

FIGURE 7 Role of regularization factor.

Along with the role of bead density or correlation threshold, we studied the error in force determination by changing the regularization factor over two orders of magnitude (right panel). As predicted by simulations (left panel), the error in force is almost independent of this factor except at low bead density (less than 1.5 bead per interrogation window). Again, this is consistent with the results presented in Figures 4 and 5 and confirms the choice of four beads per window as optimal bead density in displacement and force measurement.

4. PREPARATION OF PATTERNED POLYACRYLAMIDE GELS WITH FIDUCIAL MARKERS

The preparation of patterned polyacrylamide hydrogels is performed in three steps (Figure 8):

- coating of 24 × 24 mm glass coverslips with ECM,
- silanization of 20 × 20 mm glass coverslips, and
- polymerization of polyacrylamide hydrogels in between the ECM-coated coverslip and the silanized coverslip.

4.1 MATERIALS

- Silane solution: (3-(Trimethoxysilyl)-propyl-methacrylate) (Cat. N° M6514; Sigma–Aldrich, USA) in milliQ water, containing 2.0% v/v Ethanol
- Phosphate buffered saline (PBS) (Cat. N° 10010-023, Invitrogen, France)
- Glass coverslips 20 × 20 mm and 24 × 24 mm (Knittek glass, Germany)
- Acrylamide solution (Cat. N° 01697, Fluka Analytical, USA)
- *N*,*N*′,methylenebisacrylamide solution (Cat. N° 66675, Fluka Analytical, USA)
- TEMED (*N*,*N*,*N*′,*N*′-Tetramethylethylenediamine, (Cat. N° T9281, Sigma–Aldrich, USA)
- Ammonium persulfate (APS) (Cat. N° A3678, Sigma–Aldrich, USA)
- Collagen type-I in solution (Cat. N° 354236, BD Bioscience, USA)
- Fibronectin in solution (Cat. N° F1141, Sigma–Aldrich, USA)
- Acetic acid (Cat. N° A6283, Sigma–Aldrich, USA) 0.2% v/v in milliQ water
- Fluorescent nanobeads (580/605): Carboxylated modified microspheres 0.2-μm diameter (Cat. N° F8810, Invitrogen, USA)

4.2 EQUIPMENT

- Oxygen plasma cleaner (FEMTO, Diener electronics)
- Oven

4.3 COATING OF 24 × 24 MM GLASS COVERSLIPS WITH ECM

- A 24 × 24 mm glass coverslip is oxidized in the oxygen plasma cleaner (FEMTO, Diener electronics) at 30 W for 30 s.
- Alternatively the glass coverslip can be simply cleaned with acetone and then ethanol.
- A 100 μL droplet of fibronectin (and possibly collagen) at 40 μM in PBS is placed on a piece of parafilm and then covered with the clean glass coverslip.
- After 30 min, detach the coverslip from parafilm by carefully injecting 1000 μL of PBS between the parafilm and the coverslip and taking the coverslip with tweezers. Wash once in PBS and let dry.

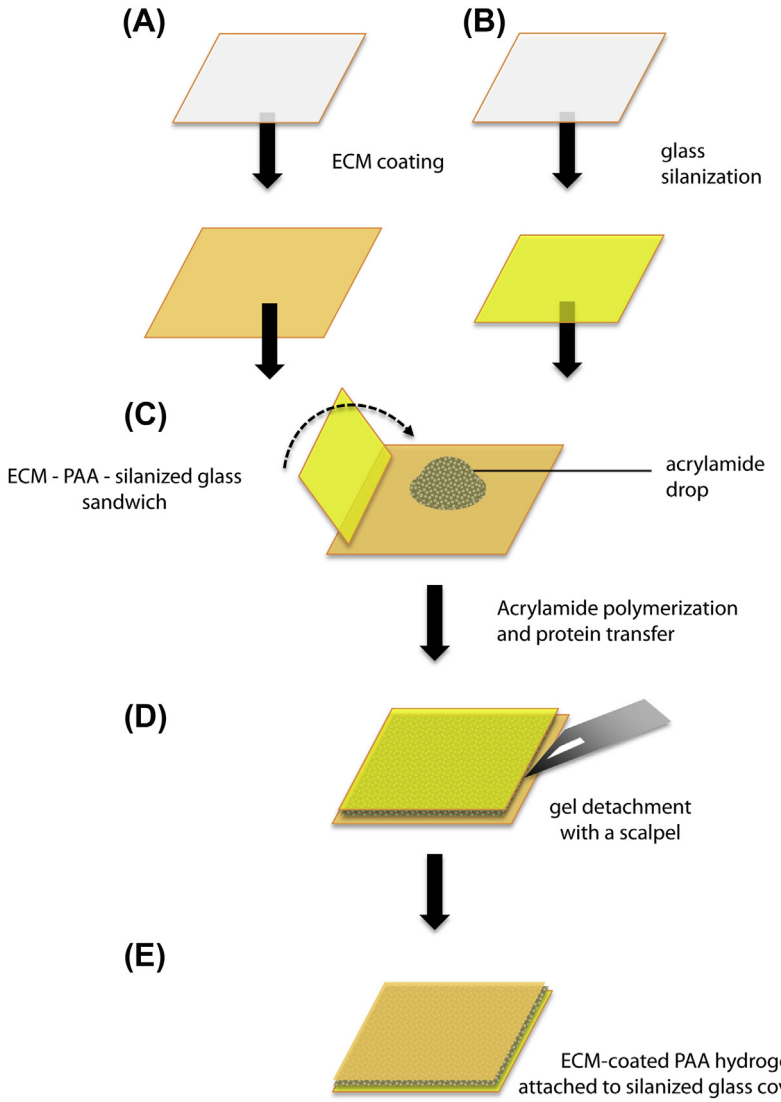

FIGURE 8 Preparation of ECM-coated polyacrylamide hydrogels.

A glass coverslip, 24 × 24 mm, is coated with ECM proteins (A). A glass coverslip, 20 × 20 mm, is silanized (B). A drop of acrylamide/bisacrylamide mixture is sandwitched between the ECM-coated and the silanized coverslips (C). After 30 min polymerization, the silanized coverslip is detached with a scalpel (D). The ECM proteins remain attached to the polyacrylamide gel onto the silanized coverslip (E).

4.4 SILANIZATION OF 20 × 20 MM GLASS COVERSLIPS

- Wash 20 × 20 mm coverslips by immersion in water and then in ethanol (few seconds each). Dry the coverslips with pressurized air (few seconds).
- Activate the 20 × 20 mm coverslips with Plasma (3 min, 100 W).
- Immerse the coverslip for 10 min in the silanization solution: 2% v/v of (3-(Trimethoxysilyl)-propyl-methacrylate) and 1% v/v of acetic acid in ethanol 96%. Owing to the toxicity of this particular step, this procedure must be carried out under a chemical hood.
- After silanization of the glass surface, coverslips are washed twice with ethanol (few seconds), followed by drying with pressurized air.
- Silanized coverslips are placed in a warm oven (120 °C) for 1 h.
- Coverslips can then be kept at room temperature and used within 1 month.

4.5 POLYMERIZATION OF POLYACRYLAMIDE

- Mix acrylamide and bisacrylamide in the proportions indicated by Tse and Engler (2010) in order to obtain the appropriate stiffness. A ratio of 5%/0.225% for acrylamide/bisacrylamide leads to a gel stiffness close to 10 kPa.
- Degas acrylamide/bisacrylamide solution for at least 20 min. This procedure can be performed within a desiccator, connected to a vacuum pump.
- Add and mix 5 µl of the nanobeads solution to 160 µl of acrylamide/bisacrylamide solution.
- This mixture is immersed in an ultrasonic bath for 10 min to ensure perfect homogenization of the bead−polymer mix.
- Mix 165 µL of the bead/acrylamide/bisacrylamide solution with 1 µL of *N*,*N*,*N*′,*N*′-tetramethylethylenediamine (TEMED), and 1 µL of APS. This procedure should be performed *fast* but *carefully*, in order to avoid polymerization of the solution in the recipient and the generation of air bubbles, which could perturb polyacrylamide polymerization.
- *As fast as possible*, put 25 µl of the mix acrylamide/bisacrylamide/nanobeads/TEMED/APS at the center of the 24 × 24 mm ECM-coated coverslips.
- Cover with a 20 × 20 mm silanized coverslip, generating a sandwich-like configuration, where the bead−polyacrylamide solution will gel between the two coverslips. Avoid generation of air bubbles in the gel during contact formation. Gelation will take 30 min.
- To avoid drying of the hydrogel during gel formation, put the coverslip sandwich in a hermetic box containing a small volume of hot water (100 °C) to keep humidity high. Typically we use 10 mL of boiling water in a box of 25 × 25 × 3 cm.
- Coverslips are separated with a scalpel. The difference in size helps coverslips separation. ECM got transferred onto the polyacrylamide gel, which remained attached to the silanized coverslip due to covalent bounds formed with the acrylate groups. The 24 × 24 mm glass coverslip is discarded. ECM-coated polyacrylamide hydrogels on 20 × 20 mm glass coverslips can be stored in a PBS buffer at 4 °C, for 2 days.

5. IMAGE ACQUISITION

It is assumed that images, with fluorescent beads as markers, are obtained in conditions *with* and *without* the source of force, here the cell. In addition, gel deformation is due to the cell only and not to the treatment used for cell removal (typically trypsin digestion of cells) or to random bead motion inside the gel. Typically, stacks of five images, separated by a distance of 0.5 μm in the Z direction, are taken for both conditions (*with* and *without* force), at the same position. The first image corresponds ideally to the top of the gel, where the cell settles. During pair creation, in which an image *without* force is associated with an image *with* force, it is critical to select images in each five-image stack for which the displacement is due to the traction force exerted by the cell only. In particular, individual beads should be identifiable: the apparition of a new bead (e.g., a change of the focus) would result in spurious large displacement without physical meaning.

Finally, one assumes that the gel rigidity (Y in Eqn (2)), which can be controlled experimentally, is adapted to the expected magnitude of the force developed by cells.

- Prior to any use of PIV-FTTC plug-in, create pairs made of *without* and *with* cells images. The image *without* cells gives the reference position for beads; this image is always the first image in the pair. Pairing is crucial and beads should be identifiable in both images.
- Image stacks should be saved as tiff images (".tif" extension) in a folder (only stack images are present).
- It is assumed that the pair names have the following structure "XXX_YYY_BeadTag_ZZZ.tif." Use only "_" to separate subfields in the name. One of the subfield is the tag for bead channel (e.g. "TxRed").

6. IMAGE ANALYSIS, ESTIMATION OF DISPLACEMENT, AND TRACTION FORCE FIELDS

6.1 PREPARATION OF IMAGEJ SOFTWARE

The macro we wrote is based on few ImageJ plug-ins: *slice alignment*, *PIV*, and *FTTC*. They can be downloaded from https://sites.google.com/site/qingzongtseng/imagejplugins and installed along with your ImageJ or Fiji distribution (1.49b distribution, May 2014).

6.2 GENERATION OF THE PARAMETER FILE

ImageJ is used to run plug-ins and macro on a series of stacks of two images (see Section 5). Both PIV and FTTC methods use parameters that should be carefully adapted to specific conditions (gel rigidity, cell line, etc.). Therefore, the macro *GenerateParameterFile.ijm* is used to generate a parameter file that contains all relevant parameters for PIV or FTTC. It is designed to generate a text file containing the

required parameters for force analysis, which depends on the actual images to be analyzed, the experimental conditions, and the nature of the cell line. The generated file ("Parameters.txt") can be edited and modified for a further use without rerunning *GenerateParameterFile.ijm*.

See the supplemental text online to visualize the steps that are described below.

1. Open ImageJ (or Fiji); open macro *GenerateParameterFile.ijm*; run it (Figure S1.1).
2. Open the folder that contains all the pairs images prepared in step 0 (Figures S1.2 and S1.3).
3. Because the global error is highly dependent on the actual bead density, open a typical pair image to estimate this parameter.
4. Adjust the threshold so that the number of individual beads in the image can be measured (this step uses "Analyze Particles" ImageJ plug-in).
5. Enter the relevant values for parameters, in particular the pixel size (in micrometers) and the Young modulus of the gel (Engler et al., 2004). The Poisson ratio, which controls incompressibility parameter in equations, should be set to 0.5. The number of beads per window in the PIV analysis should be greater than 4 (or equal).
6. The next step presents the optimal combination of parameters for the PIV method, given the bead density (step 4) and the threshold (step 5). It is not recommended to modify these values.
7. Provide the relevant information for the pairs to be analyzed. Only pairs that include the bead channel in their name (enclosed by "_-.") will be analyzed.
8. Enter the number of channels. At least one channel identification tag (the bead tag) should be given.
9. Give the actual channel tag (e.g., "TxRed") and its name ("Bead"). If the bead tag is not listed, choose "other." You will be asked to provide the actual bead tag and name.
10. End of "Parameters.txt" generation. A new "ParameterData" folder is created, which contains the file "Parameters.txt." This file can be edited and/or modified for a further use without rerunning macro *GenerateParameterFile.ijm*.

6.3 MEASUREMENT OF THE CELL TRACTION ENERGY

See the supplemental text online to visualize the steps that are described below.

1. Open ImageJ (or Fiji); open macro *AlignCropPIVForce.ijm*; run it.
2. Open the folder containing (1) the list of image pairs and (2) the *ParameterData* folder.
3. First, the two images in each stack need to be aligned using the *Template Matching/Align Slices in stack* ImageJ plug-in. Select a roi (rectangle) in the first image of the pair.
4. Check the alignment by moving the image cursor at the bottom of the stack and then click "ok."

5. If alignment is correct, click "yes." The same roi will be used throughout the whole set of pairs to be aligned. If alignment is incorrect, click "no" and select a new roi; the plug-in *alignment* using the new roi is run.
6. After alignment of all pairs, crop the images; click "ok" and select the crop window.
7. After force measurement is complete, an average force map pops up (Figure 2.10). By selecting a roi (elliptic roi), the elastic energy is computed over the spatial domain including the cell.
8. Energy data (whole image or limited to the mask, see step 7) are given in "Energy_force.txt" and "Energy_forces_Mask.txt."
9. All aligned cropped images are stored in "AlignCroppedPairs." Alignment data, alignment, and the crop mask are stored in "ParameterData" folder.
10. Displacement (uses *PIV* plug-in) and force determination (uses *FTTC* plug-in) data (text file and images) are stored in "PIV_force" folder. End of force traction measurement.

6.3.1 Displacement and force vectors

Displacement and force measurement data, stored in "PIV_force" folder, come as text files or "tif" images. Text files are editable; the two first columns give the point in the image (using pixels as coordinate); the third and fourth columns give the horizontal and vertical components of displacement or force; the fifth column provides the displacement or force magnitude. Displacement is given in micrometers (10^{-6} m), whereas the force is defined as the traction force over the PIV interrogation window (window size *vs*3; actual window area $A = (vs3 \times pixel2micron)^2$); therefore, numbers in columns 3–5 (force text file) are given in pPa (10^{-12} Pa). The actual traction force (in N) is obtained by multiplying columns 3–5 by the area factor A.

6.3.2 Mechanical energy stored in gel deformation

This elastic energy is estimated by summing the dot products of displacement (columns 3 and 4, displacement text files) with the force (columns 3 and 4, force text files) times the area of the last PIV interrogation window. Displacements are given in micrometers and forces in newtons (after scaling the force vector with the area of the last interrogation window used in PIV expressed in meters). The elastic energy is given in joules.

CONCLUSION

The measurement of forces developed by cells relies on the deformation of elastic polyacrylamide gels with embedded fiducial markers. Ideally, the determination of the force map amounts to solve the nonlinear equations for the continuum mechanics, including all experimental features (heterogeneity and/or finite thickness of the gel, large deformation, intercell distance, etc.) with the help of numerical simulations (finite element methods, large and complex computer code) (Dembo &

Wang, 1999). Fortunately, it became clear during the last decade that the deformation of elastic gels driven by cell forces can be accounted for by linear mechanics and that the Boussinescq solution is enough to invert Eqn (1) (Butler et al., 2002; Sabass et al., 2008). This method gives robust and reliable 2D maps of the force exerted by cells on elastic gels.

This method is also versatile, for example, in studies on confluent cells moving collectively (Trepat et al., 2009). In this case, the closeness of cells and the finite size of the gel hinder the direct use of Eqns (1) and (2). Therefore, they adapted the physical model and the FTTC method to account for the specificities of their experimental setup (Serra-Picamal et al., 2014 [Chapter 17 of this volume]).

Force mapping can be also simply achieved using the technique of micropillars (Du Roure et al., 2005; Gupta et al., 2014; Tan et al., 2003). The mechanical probe consists in elastic micropillars, whose deflection gives the intensity of the force with which the cell is pulling. In this approach, the physical model uses pillar elasticity and density to relate the pillar bending to the force exerted by cells. The advantage is that computation step to deduce forces from pillar bending is extremely simple, since pillars are considered elastic and independent. The drawback is that surface microstructure may affect cell adhesion and bias cell behavior.

Here, we simplify the classical traction force microscopy computation step by sharing new ImageJ macros and former plug-ins developed in our group (Tseng et al., 2011, 2012) to offer the possibility to new incomers to measure cell traction forces without the need for particular expertise. Our model for the displacement−force relationship is linear (Eqn (1)) and, assuming small deformation for the gel, the kernel used in Eqn (1), is the Boussinescq solution, valid for a semi-infinite space. This analysis is runnable on personal computers equipped with ImageJ (or Fiji) with the help of plug-ins (download from https://sites.google.com/site/qingzongtseng/imagejplugins) and macros presented in this study. It offers the possibility to analyze the mechanical response of cells (or groups of two cells) in response to chemical drugs or geometrical constraints via micropatterned substrates (Tseng et al., 2011, 2012). In conclusion, our work makes cell traction force measurement amenable to daily routine in any biology laboratory.

SUPPLEMENTARY DATA

Supplementary data related to this chapter can be found at http://dx.doi.org/10.1016/bs.mcb.2014.10.008.

REFERENCES

Butler, J. P., Tolić-Nørrelykke, I. M., Fabry, B., & Fredberg, J. J. (2002). Traction fields, moments, and strain energy that cells exert on their surroundings. *American Journal of Physiology − Cell Physiology, 282*, C595−C605.

Dembo, M., & Wang, Y. (1999). Stresses at the cell-to-substrate interface during locomotion of fibroblasts. *Biophysical Journal, 76*, 2307−2316.

Du Roure, O., Saez, A., Buguin, A., Austin, R. H., Chavrier, P., Silberzan, P., et al. (2005). Force mapping in epithelial cell migration. *Proceedings of National Academy of Sciences USA, 102*, 2390−2395.

Engler, A., Bacakova, L., Newman, C., Hategan, A., Griffin, M., & Discher, D. E. (2004). Substrate compliance versus ligand density in cell on gel responses. *Biophysical Journal, 86*, 15−25.

Gupta, M., Kocgozlu, L., Sarangi, B. R., Margadant, F., Ashraf, M., & Ladoux, B. (2015). Micropillar Substrates: a tool for Studying Cell Mechanobiology. *Methods in Cell Biology, 125*, 289−308.

Kopansaka, K. S., Bussonier, M., Geraldo, S., Simon, A., Vignjevic, D., & Betz, T. (2015). Quantification of collagen contraction in three-dimensional cell culture. *Methods in Cell Biology, 125*, 353−372.

Pelham, R. J., & Wang, Y. (1997). Cell locomotion and focal adhesions are regulated by substrate flexibility. *Proceedings of National Academy of Sciences USA, 94*, 13661−13665.

Plotnikov, S. V., Sabass, B., Schwarz, U. S., & Waterman, C. M. (2014). *High-resolution traction force microscopy.* Elsevier Inc.

Rape, A. D., Guo, W.-H., & Wang, Y.-L. (2011). The regulation of traction force in relation to cell shape and focal adhesions. *Biomaterials, 32*, 2043−2051.

Sabass, B., Gardel, M. L., Waterman, C. M., & Schwarz, U. S. (2008). High resolution traction force microscopy based on experimental and computational advances. *Biophysical Journal, 94*, 207−220.

Schiller, H. B., Hermann, M.-R., Polleux, J., Vignaud, T., Zanivan, S., Friedel, C. C., et al. (2013). β1- and αv-class integrins cooperate to regulate myosin II during rigidity sensing of fibronectin-based microenvironments. *Nature Cell Biology, 15*, 625−636.

Serra-Picamal, X., Conte, V., Sunyer, R., Muñoz, J. J., & Trepat, X. (2015). Mapping forces and kinematics during collective cell migration. *Methods in Cell Biology, 125*, 309−330.

Stricker, J., Sabass, B., Schwarz, U. S., & Gardel, M. L. (2010). Optimization of traction force microscopy for micron-sized focal adhesions. *Journal of Physics: Condensed Matter, 22*, 194104.

Tambe, D. T., Croutelle, U., Trepat, X., Park, C. Y., Kim, J. H., Millet, E., et al. (2013). Monolayer stress microscopy: limitations, artifacts, and accuracy of recovered intercellular stresses. *PLoS One, 8*, e55172.

Tan, J. L., Tien, J., Pirone, D. M., Gray, D. S., Bhadriraju, K., & Chen, C. S. (2003). Cells lying on a bed of microneedles: an approach to isolate mechanical force. *Proceedings of National Academy of Sciences USA, 100*, 1484−1489.

Trepat, X., Wasserman, M. R., Angelini, T. E., Millet, E., Weitz, D.a., Butler, J. P., et al. (2009). Physical forces during collective cell migration. *Nature Physics, 5*, 426−430.

Tse, J. R., & Engler, A. J. (2010). Preparation of hydrogel substrates with tunable mechanical properties. Current Protocol in Cell Biology. *Supplement, 47*. unit 10.16.

Tseng, Q., Duchemin-Pelletier, E., Deshiere, A., Balland, M., Guillou, H., Filhol, O., et al. (2012). Spatial organization of the extracellular matrix regulates cell-cell junction positioning. *Proceedings of National Academy of Sciences USA, 109*, 1506−1511.

Tseng, Q., Wang, I., Duchemin-Pelletier, E., Azioune, A., Carpi, N., Gao, J., et al. (2011). A new micropatterning method of soft substrates reveals that different tumorigenic signals can promote or reduce cell contraction levels. *Lab on a Chip, 11*, 2231−2240.